IEEE Access
Multidisciplinary | Rapid Review | Open Access Journal

Received November 12, 2018, accepted December 18, 2018, date of publication January 1, 2019,
date of current version January 16, 2019.

Digital Object Identifier 10.1109/ACCESS.2018.2889992

Screen Content Image Quality Assessment With Edge Features in Gradient Domain

RUIFENG WANG, HUAN YANG, (Member, IEEE), ZHENKUAN PAN, BAOXIANG HUANG, AND GUOJIA HOU

College of Computer Science and Technology, Qingdao University, Qingdao 266071, China

Corresponding author: Huan Yang (cathy_huanyang@ hotmail.com)

This work was supported in part by the National Natural Science Foundation of China under Grant 61602269, in part by the Application Research Funding of Qingdao under Grant 2016025, and in part by the China Postdoctoral Science Foundation under Grant 2017M622136.

ABSTRACT Objective visual quality assessment specific for screen content images (SCIs) has been increasingly investigated over the years. In this paper, an effective full-reference quality evaluation model for SCIs is proposed, in which edge features in gradient domain (EFGD) are extracted for better visual perceptual representation. Unlike traditional edge feature extraction directly in the image pixel domain, all edge features in the proposed EFGD model are extracted based on the gradient map of input SCIs, including edge sharpness, edge brightness/contrast, and edge chrominance. Specifically, the gradient profile model that can well represent the spatial layout of edges is adopted to measure the edge sharpness degree. A novel computation way is reported to measure the edge brightness and contrast change between the reference and distorted SCIs, while color moments are used to account for the color chrominance variation. In addition, an adaptive weighting strategy is designed to adjust the effects of these three kinds of edge features, according to the statistical distributions of the input SCIs. Moreover, the maximum value of edge sharpness features is extracted from the test SCIs as the pooling weight to get the final image quality assessment (IQA) score. The experimental results on two commonly used SCIs databases have verified the superiorities of the EFGD model and show that the EFGD model is in more conformity with the subjective assessment results than most of the existing IQA models.

INDEX TERMS Image quality assessment, screen content image, edge feature, gradient domain.

I. INTRODUCTION

The content of digital images is no longer confined to natural scene images (NSIs) in intelligence information processing. In fact, today's digital images come from many sources, which combine texts, charts and natural scenes in various layouts, and have been increasingly applied in many intelligent communication applications, such as virtual screen sharing, online news and advertising, online education, electronic brochures, remote computing, cloud computing and so on. This kind of images viewed on computer is called screen content images (SCIs) [1], [2]. The results in [3] show that SCIs have different images characteristics compared with NSIs. Such images tend to have unique characteristics, such as sharp edges, dense intensity variation and limited colors in specific areas. In processing of SCIs (e.g., generation, compression and transmission), all kinds of distortion (e.g., blurring, color saturation change, contrast change, compression) will inevitably lead to image quality degradation. Therefore, how to accurately evaluate visual quality of SCIs is of great significance.

A key problem related to image quality assessment (IQA) of SCIs is: how to evaluate the image quality objectively and ensure that the measurement derived from the designed objective model has high consistence with judgment of the human visual system (HVS). The most simple objective IQA models are peak signal-to-noise ratio (PSNR) and mean square error (MSE). However, compared with the HVS, these two models often lead to inconsistent perceptual results. Because PSNR and MSE only take the difference between the pixel intensity into account [4], [5]. In order to settle this question, great efforts have been made to introduce the characteristics of the HVS into the construction of IQA models. A milestone paper is the structural similarity measure (SSIM) [5], which considers local luminance, contrast and structure degradation, not just the difference in pixel intensity. To further improve the performance of SSIM, lots of objective models are designed,

such as, feature similarity (FSIM) [6], gradient similarity (GSIM) [7], and information weighted SSIM (IW-SSIM) [8].

Further considering that image content with sharp edges and contours is more sensitive to the HVS, many methods focus on edge information extraction for the construction of IQA models [9]–[11]. By the computation of the similarity of edge strength, the model (ESSIM) is proposed in [9]. Xue *et al.* [10] proposed a gradient magnitude similarity deviation (GMSD) model for IQA, which only use the gradient magnitude similarity to represent the quality of images, and the complexity of this model is very low. In [11], an efficient full reference IQA model is proposed, called mean deviation similarity index (MDSI), in which gradient similarity, chromaticity similarity and deviation pooling are measured. Perceptual features are also applied to image quality assessment models. Zhang *et al.* [12] reported a visual saliency based full reference IQA method, named visual saliency-based index (VSI). Sheikh and Bovik [13] proposed a visual information fidelity measure for IQA, called visual information fidelity (VIF). In [14], natural scene statistics (NSS) is explored for image fidelity measure. In [15], based on NSS, the authors present a specific quality metric for blurring images. Gao *et al.* [16] used different kinds of statistic features in IQA model development, such as mean subtracted contrast normalized features, the gradient magnitude features and the Laplacian of Gaussian features. Besides, various computational methods are also introduced into IQA model design, such as multi-scale analysis [17], kernel learning [18], support vector regression [19], extreme learning machine [20] and deep learning [21]–[27].

Most of these IQA models are proposed to evaluate the perceived quality of NSIs. Obviously, these models are more appropriate for evaluating NSIs than for evaluating the quality of SCIs because the image structure and statistical properties of SCIs are usually very different from those of NSIs [1].

Many objective quality assessment models specific for SCIs are reported since then. Yang *et al.* [1] proposed a model (SPQA) by considering the visual differences between text and pictorial regions in SCIs and constructed the first SCI image quality assessment database (SIQAD). Wang *et al.* [28] considered the visual field adaptation of structural similarity and the weight of information content in local quality evaluation, and proposed a model (SQI). Gu *et al.* [29] proposed a model (SIQM) which works with a weighting strategy based on the structural degradation measurement. Ni *et al.* [30] used three kinds of edge features extracted from SCIs in the developed edge similarity (ESIM) model. They also developed a new database called SCID for quality assessment of SCIs in [30]. Fang *et al.* [31] proposed a model by structure features and uncertainty weighting (SFUW), considering different influences of image patches on calculation of quality scores of SCIs. Ni *et al.* [32] also proposed an effective full reference image quality assessment model, named Gabor feature model (GFM), which was established based on the horizontal and vertical imaginary-part Gabor features.

In view of efforts of above methods, we propose a novel objective IQA model based on edge feature extraction in gradient domain, named EFGD, to further improve the quality prediction accuracy for SCIs. The edge features extracted in gradient domain can well reflect the visual quality of SCIs. Three basic edge feature maps, i.e. edge sharpness map (ESM), edge brightness contrast map (EBCM) and edge chrominance map (ECM) are extracted in gradient domain of SCIs. The edge sharpness and brightness/contrast features are computed based on the luminance channel of input images, while the edge chrominance is based on the chrominance channels. Gradient profile sharpness (GPS) model [33] is adopt to measure the edge sharpness in this manuscript. Furthermore, a novel computation method is proposed to capture the brightness and contrast variation of the gradient map (i.e., edge brightness/contrast). Chroma information also plays a crucial role in the edge perception of SCIs, so we exploited color moments [34] of chrominance channels in gradient domain to represent edge chrominance. The similarities of these three kinds of edge features between original and distorted SCIs are computed respectively, and are finally fused based on the proposed adaptive weighting strategy. The edge sharpness feature is also used as a pooling map to convert the fused similarity map to a final quality score of the distorted SCI. Compared with previous IQA models, the proposed EFGD model has the following main contributions:

(1) Unlike generic edge feature extraction directly from image pixel domain, we firstly extract edge features in gradient domain, which can well reflect the prominent visual changes in distorted SCIs.
(2) Gradient profile model is implemented to measure the edge sharpness feature, which can better represent the details of edge in SCIs. The proposed feature extraction of edge brightness/contrast also plays important role in improving the performance of the model.
(3) An adaptive weighting algorithm is designed according to the statistical distribution of images, which adjusts the fusion weights of the three similarity maps.
(4) The EFGD model achieves the highest overall performance on two commonly used verification databases: SIQAD and SCID.

The other contents of this paper are as follows. In section II, the proposed EFGD model is introduced in detail. Test results of the proposed IQA model on the two databases and comparison with other latest IQA models are reported in section III. Finally, Section IV draws a conclusion of the manuscript.

II. PROPOSED EFGD MODEL FOR SCI QUALITY ASSESSMENT

Generally speaking, an ideal image quality assessment model should be highly consistent with the HVS perception.

The main concern of the proposed IQA model is how to extract effective image features in SCIs. We hope that these features can better describe the perception of HVS. Since screen images contain rich edge details, and the HVS is highly

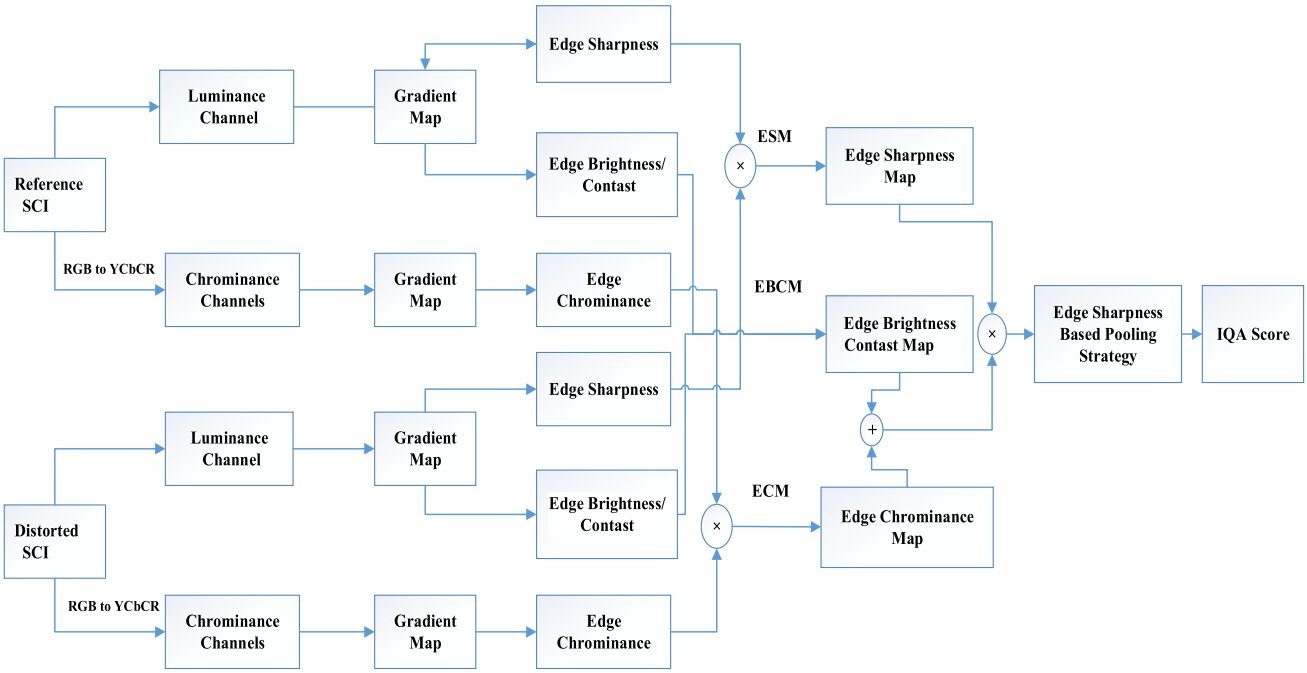

FIGURE 1. Framework of the proposed EFGD algorithm.

sensitive to image edges, we try to extract effective edge features based on which a better assessment metric can be constructed. Different from traditional edge feature extractions usually designed in image pixel domain, gradient-domain features of edges are investigated in quality assessment of SCIs in this manuscript. The framework of the proposed EFGD model is shown in Fig. 1, and it contains the following stages:

(1) *Chromaticity Space Conversion:* Reference and distorted SCIs are converted from *RGB* color space to *YCbCr* color space for separating their luminance channels and chrominance channels.
(2) *Edge Feature Extraction in Gradient Domain:* For the luminance channel and chrominance channels of SCIs, three edge features are extracted on the gradient map: edge sharpness, edge brightness/contrast and edge chrominance.
(3) *Similarity Measurement:* In the process of obtaining the final similarity map, we fuse the ESM, EBCM and ECM through the proposed adaptive weighting algorithm.
(4) *Pooling Strategy:* The final IQA score is obtained by pooling the final similarity map with the edge sharpness based pooling strategy.

Next, we will give the details of the proposed model.

A. CHROMINANCE SPACE CONVERSION AND CALCULATION OF GRADIENT MAP

In this work, edge features are extracted based on the luminance channel and the chrominance channel separately. Input SCIs are firstly converted from the *RGB* color space to the *YCbCr* color space according to the Eq. (1), so that the luminance channel and the chrominance channels are separated.

$$\begin{bmatrix} Y \\ Cb \\ Cr \end{bmatrix} = \begin{bmatrix} 0.2990 & 0.5870 & 0.1140 \\ -0.1428 & -0.2910 & 0.4392 \\ 0.4392 & -0.3678 & -0.0714 \end{bmatrix} \begin{bmatrix} R \\ G \\ B \end{bmatrix} + \begin{bmatrix} 0 \\ 16 \\ 128 \end{bmatrix} \tag{1}$$

In Eq. (1), *RGB* represent the three-color channels of input images, and Y, Cb and Cr denote the luminance and two chrominance channels of SCI.

In this paper, one-dimensional Gaussian function is firstly used to perform low-pass filtering on the image by row and column respectively. The Gaussian function is:

$$f(x) = \frac{1}{\sqrt{2\pi}a} \exp(-\frac{x^2}{2a^2}) \tag{2}$$

where a represents the standard deviation in the Gaussian function.

Since edge features are extracted in gradient domain in the proposed EFGD model, the gradient map of the luminance channel is firstly calculated via Eq. (3) and (4). The gradient magnitude and the gradient directions of each point in the smoothed luminance image $I(x, y)$ are calculated. The partial derivatives of horizontal and vertical direction are computed according to Eq. (3), which calculate the finite difference of the first order partial derivative in the

surrounding 2×2 window.

$$\begin{aligned} &G_h(x,y) \\ &= \frac{I(x+1,y) - I(x,y) + I(x+1,y+1) - I(x,y+1)}{2} \\ &G_v(x,y) \\ &= \frac{I(x,y+1) - I(x,y) + I(x+1,y+1) - I(x+1,y)}{2} \end{aligned} \tag{3}$$

where $G_h(x,y)$, $G_v(x,y)$ denote the derivatives in horizontal and vertical directions. These two terms are used to calculate the gradient magnitude $G(x,y)$ and the gradient direction $\vec{F}(x,y)$. The $G(x,y)$ is defined as the summary of the absolute values of $G_h(x,y)$ and $G_v(x,y)$:

$$G(x,y) = |G_h(x,y)| + |G_v(x,y)| \tag{4}$$

The gradient direction is calculated as Eq. (5):

$$\vec{F}(x,y) = \arctan(G_h(x,y)/G_v(x,y)) \tag{5}$$

We note the gradient map of the luminance channel as $G_L(x,y)$. Gradient maps of the two chrominance channels (Cb and Cr) are also computed according the Eq. (3) and (4).

B. EXTRACTION OF EDGE FEATURES IN GRADIENT DOMAIN

The construction of the three similarity maps (i.e., ESM, EBCM and ECM) is introduced in this section. The detailed algorithms are given below.

1) EDGE SHARPNESS MAP (ESM) AND GRADIENT PROFILE SHARPNESS(GPS)

Edge represents the outline of images and has rich details. Edges in SCIs are generally narrow and sharp [2]. So, how to measure edge sharpness is a very important work. Therefore, we consider using the Gradient Profile Sharpness (GPS) [33] to express the edge sharpness. GPS uses gradient profiles to describe the spatial layout of image gradients, where each gradient profile is defined as a 1-D profile of gradient magnitudes across an edge pixel in the direction of the gradient.

In GPS, the zero-crossing pixels are denoted as edge pixels, which are the local maximum on their gradient directions. Non-maximal suppression [35] is performed on the gradient map of the luminance channel to determine candidate edge pixels. In the process of non-maximum suppression, gradient magnitude of each pixel in $G_L(x,y)$ is compared with its two adjacent points in the gradient direction. If the gradient magnitude of this point is smaller, it indicates that the point is not a local maximum i.e., the point is not an edge pixel. Otherwise, this point is an edge pixel.

After edge pixels are obtained, the gradient profile is then determined. If a pixel p_0 is an edge pixel, beginning from p_0 we trace a 1-D path along its gradient direction (both sides) one by one until the gradient amplitude is no longer reduced. We call this 1-D path as a *gradient profile*, and denote the set of all the traced pixels as p_ψ, $\psi \in \{\ldots -2, -1, 0, 1, 2 \ldots\}$.

We use the gradient profile sharpness (GPS) to express the edge sharpness (ES)

$$ES(x,y) = \sqrt{\sum_{p \in p_\psi} m'(p) \cdot d^2(p, p_0)} \tag{6}$$

where $m'(p) = \frac{m(p)}{\sum_{s \in p_\psi} m(s)}$ and $d(p, p_0)$ denote the length between the edge pixel p_0 and one of its adjacent pixel p.

Finally, the edge sharpness of the reference SCI and the distorted SCI is merged to express the edge sharpness map (ESM), and the calculation method is as follows:

$$ESM(x,y) = \frac{2ES_r(x,y) \cdot ES_d(x,y) + T_s}{ES_r^2(x,y) \cdot ES_d^2(x,y) + T_s} \tag{7}$$

where $ES_r(x,y)$, $ES_d(x,y)$ denote the edge sharpness of the reference SCI and the distorted SCI respectively. T_s is a constant greater than 0, which is introduced to prevent the denominator molecule from appearing as zero or minimum value to cause instability.

2) EDGE BRIGHTNESS CONTRAST MAP (EBCM)

SCIs are usually directly rendered by computer. The brightness and contrast variation of different displays easy lead to distortion of the SCI. We think about how to extract the edge brightness and contrast feature of the SCI in the gradient domain. We used a 7x7 Gaussian weighting function $W = \{\omega_i | i = 1, 2, 3 \ldots\ldots N\}$ with standard deviation of 7/6, normalized to unit $\sum_{i=1}^{N} \omega_i = 1$ to find the local mean value, standard deviation and covariance.

Firstly, the edge brightness variation (EBV) of the reference SCI and the distorted SCI is calculated on the $G_L(x,y)$:

$$EBV(x,y,) = e^{-\left|\frac{\mu_{gr} - \mu_{gd}}{L}\right|} \tag{8}$$

where L = 255 represents the dynamic range of the pixel value, $\mu_{gr}(x,y)$ and $\mu_{gd}(x,y)$ indicate the mean of gradient map of the reference SCI and the distorted SCI respectively.

In addition, from the perspective of the HVS, too large contrast may result in loss of structural details, while too small contrast will also make the image hierarchical perception worse [36]. Hence, contrast is also a key factor in evaluating the quality of SCIs. Edge contrast variation (ECV) can describe the similarity of the contrast between the reference SCI and the distorted SCI.

$$ECV(x,y) = \ln(1 + \frac{\sigma_{rd}(x,y) + T_l}{\sigma_{gr}^2(x,y) + T_l}) \tag{9}$$

where σ_{gr} is the variance of the reference SCI luminance channel gradient domain and σ_{rd} is the covariance of the SCI and distortion SCI luminance channel gradient domain. T_l is a constant as T_s which is greater than zero.

Finally, the edge brightness contrast map (EBCM) of SCI is calculated by combining the edge brightness change with the edge contrast change. The calculation of the EBCM is as Eq. (10).

$$EBCM(x,y) = [EBV(x,y)]^{\lambda} \cdot [ECV(x,y)]^{1-\lambda} \tag{10}$$

FIGURE 2. A illustration edge features in Gradient domain of SCIs: [Column 1]: (a) a reference SCI. (b) SCI with Gaussian blur (c) SCI with contrast change. (d) SCI with JPEG2000 compression [Column 2] their Gradient Profile Sharpness (GPS) [Column3 and 4] their Edge Brightness and contrast features in gradient domain respectively.

where λ is used to adjust the relative weight between $EBV(x, y)$ and $ECV(x, y)$. In our experiments, λ is set to 0.1.

To illustrate edge features in gradient domain from SCIs, we show the extracted edge features in Fig .2, involving three different distortion types (i.e., Gaussian blur, contrast change, and JPEG2000 compression). A reference SCI and its distorted versions chosen from the SIQAD database are shown in Fig. 2 (a), (b), (c) and (d). Their related edge sharpness

and edge brightness/contrast feature maps are illustrated in Fig.2 (a1)-(d3). From this figure, it can been seen that these three kind of features reflect different visual components. For example, comparing Fig. 2 (a1), (b1) and (c1), it is easy to find that the sharpness information loss in (c1) is worst. And the brightness and contrast change is also obvious, which indicates that edge features reflect visual information well.

3) EDGE CHROMINANCE MAP(ECM)

Considering the distortion of SCIs, chrominance distortion often occurs in addition to brightness distortion. For example, the change of color saturation is due to color rendering and screen sharing between different display devices. In the process of modeling, we also need to find a suitable way to extract chrominance information from images. As the simplest and most effective feature to describe the color information of an image, color histogram, color moments, color aggregation vectors, color sets etc. are commonly used. In our algorithm, we refer to the color moment based feature extraction [34], which uses mean value, variance and slope to express the first order moment, second order moment and third order moment of chromaticity information. Since the color distribution information is mainly amassed in the low-order moments, the first order moment is the simplest feature to describe the color information of the image. Hence, we only extract the first order moments of the gradient maps ($G_{cb}(x, y)$ and $G_{cr}(x, y)$) to represent the edge chrominance information.

First, we calculate the gradient maps of the two channels Cb and Cr for the reference SCI and the distortion SCI, i.e., $G^r_{cb}(x, y)$, $G^d_{cb}(x, y)$ and $G^r_{cr}(x, y)$, $G^d_{cr}(x, y)$. Then, we calculate their mean values and fuse them to obtain the edge similarity:

$$\mu_1(x, y) = \frac{1}{H} \sum_{(x,y\in W)} G^r_{Cb}(x, y) \tag{11}$$

$$\mu_2(x, y) = \frac{1}{H} \sum_{(x,y\in W)} G^d_{Cb}(x, y) \tag{12}$$

$$\mu_3(x, y) = \frac{1}{H} \sum_{(x,y\in W)} G^r_{Cr}(x, y) \tag{13}$$

$$\mu_4(x, y) = \frac{1}{H} \sum_{(x,y\in W)} G^d_{Cr}(x, y) \tag{14}$$

$$S_{cb}(x, y) = \frac{2\mu_1(x, y) \cdot \mu_2(x, y) + T_C}{\mu_1^2(x, y) + \mu_2^2(x, y) + T_C}$$
$$S_{cr}(x, y) = \frac{2\mu_3(x, y) \cdot \mu_4(x, y) + T_C}{\mu_3^2(x, y) + \mu_4^2(x, y) + T_C} \tag{15}$$

where W denotes the local windows and H is the size of the window. $\mu_1(x, y)\mu_2(x, y)\mu_3(x, y)$ and $\mu_4(x, y)$ denotes to the first moment of the gradient maps of the Cb and Cr channels of the reference SCI and the distorted SCI, respectively. $S_{Cb}(x, y)$ denotes the similarity of the edge chrominance of Cb channel, and $S_{Cr}(x, y)$ denotes the similarity of edge chrominance of the Cr channel. The purpose of introduction of T_c is to prevent instability.

Then, the similarity maps of edge chrominance of the two channels are combined to obtain the final edge chrominance map (ECM):

$$ECM(x, y) = S_{cb}(x, y) \cdot S_{cr}(x, y) \tag{16}$$

C. ADAPTIVE WEIGHTING STRATEGY

The proposed algorithm does not simply combine each map directly. The edge brightness contrast map (EBCM) and edge chrominance map (ECM) are combined by addition and then the edge sharpness map (ESM) is combined to get the final similarity measure. The formula is as follows:

$$S(x, y) = [\beta \cdot EBCM(x, y) + (1 - \beta) \cdot ECM(x, y)]^\theta \cdot [ESM(x, y)]^\gamma \tag{17}$$

where θ and γ are two positive constants that can control the relative importance of edge features. By treating these features equally important, $\theta = \gamma = 1$ is set in our work. For the setting of β in Eq. (17), we use the average value of the $EBCM(x, y)$ to tune the value of β. The calculation of the average value is as follows:

$$v = \frac{1}{MN} \sum_{x=1}^{M} \sum_{y=1}^{N} EBCM(x, y) \tag{18}$$

where MN is the number of pixels in EBCM. Through comparative experiments, β is set as follows:

- when $v \subset [0.31, 0.71]$, $\beta = 0.7$;
- when $v > 0.71$, $\beta = 0.3$;
- for the remaining cases, $\beta = 0.4$

D. EDGE SHARPNESS BASED POOLING STRATEGY

This section is the last processing stage, which will produce the final screen image quality score. We consider using an appropriate pooling process, rather than directly averaging the final edge similarity map $S(x, y)$, because the perception of image pixels by the human visual system is not equal. We choose the maximum value of edge sharpness extracted from luminance channel in reference SCI and distorted SCI as weighted map to measure the quality of each pixel to the whole image.

The weight map is expressed as ESW_r, ESW_d. The weight graph based on edge acuity feature is calculated as follows:

$$\omega(x, y) = \max(ESW_r, ESW_d) \tag{19}$$

Therefore, the IQA score can be computed with the weighting metric as in Eq. (20).

$$Score = \frac{\sum_{(x,y)} \omega(x, y) \cdot S(x, y)}{\sum_{(x,y)} \omega(x, y)} \tag{20}$$

III. EXPERIMENTAL RESULTS

In this section, we present and discuss the performance of our proposed EFGD quality model with 17 state-of-the-art IQA models on two image quality assessment databases designed for quality assessment of SCIs.

A. DATABASE AND ASSESSMENT CRITERIA

In our wok, two image quality databases related to SCIs are used. The first one is SIQAD [1]. It contains 20 reference and 980 distorted SCIs, which takes into account 7 distortions and 7 distortion levels for each distortion. Another is SCID [30]. It contains 1840 SCIs, including 40 reference SCIs and 1800 distorted SCIs, which uses 9 different types of image distortion to render these reference SCIs and creates 5 distortion levels for each type of distortion.

Then, we take three common methods to calculate the correlation between subjective and objective scores: SROCC (Spearman Rank-order Correlation Coeffi-cient), PLCC (Pearson Linear Correlation Coefficient), and RMSE (Root Mean Squared Error). We use SROCC to estimate the monotonicity of prediction and PLCC to measure the accuracy of forecasts. RMSE indicate the deviation between the objective and subjective scores. Finally, it should be noted that the larger the value of SROCC and PLCC denote better performance. On the contrary, a lower RMSE value denotes a better performance. The three correlation coefficients are calculated as Eq. (21), (22) and (23):

$$PLCC = \sum_{i=1}^{n}(Z_i-\overline{Z})(O_i-\overline{O}) \Bigg/ \sqrt{\sum_{i=1}^{n}(Z_i-\overline{Z})^2(O_i-\overline{O})^2} \tag{21}$$

$$SROCC = 1 - \frac{1}{n(n^2-1)}6\sum_{i=1}^{n} d_i^2 \tag{22}$$

$$RMSE = \sqrt{\frac{1}{n}\sum_{i=1}^{n}(O_i-\overline{O})^2} \tag{23}$$

where n represents the number of distorted images, d_i is the difference between the ith image's ranks in subjective and objective levels. Letters $\overline{O}$ and $\overline{Z}$ express the mean values of O_i and Z_i. O_i and Z_i are the objective and subjective scores of $i-th$ SCI in the database which has n SCIs.

Before calculating the three assessment indicators, it is necessary to eliminate the nonlinearity of objective quality prediction. According to the standard procedures as suggested in the video quality experts group (VQEG) HDTV test [37], [38], we nonlinearly return the quality score to a common space utilizing a five-parameter mapping function, as follows Eq.(24):

$$Z_i = \eta_1 + \{\frac{1}{2} - \frac{1}{1+\exp[\eta_2(s_i-\eta_3)]}\} + \eta_4 s_i + \eta_5 \tag{24}$$

where s_i is the perceived quality score of the $i-th$ distortion SCI calculated by the IQA model and z_i is the relevant mapped score. η_1, η_2, η_3, η_4 and η_5 are five parameters to be determined during the curve fitting process.

B. OVERALL PERFORMANCE COMPARISON AND ANALYSIS

To illustrate its superiority, the proposed EFGD is compared with multiple IQA models, including PSNR, SSIM [5], IWSSIM [8], VIF [13], MAD [39], FSIM (for grey image) [6], GSIM [7], GMSD [10], VSI [12], SCQI [40], SIQM [29], SPQA [1], SQI [28], SQMS [41], ESIM [30], SVQI [42] and GFM [32]. The last seven IQA models are specifically designed for the SCIs, while the rest are all for assessment of NSIs.

TABLE 1 and TABLE 2 show the overall performance of all IQA models on the SIQAD and SCID databases, respectively. In both tables, the first level performance diagram for each measurement standard (i.e., PLCC, SROCC, and RMSE) is shown in red, and all program source code for the comparison models are downloaded from the original address. Therefore, SPQA and SQI results on the SCID database and some special results on the SIQAD database are not available.

It is worth to note that there are four parameters of the proposed EFGD model. As suggested in [7] and [12], these parameter values leading to higher SROCC, will be selected.

The values of them are empirically determined as 0.3, 10, 120, and 0.1 by extensive experiments respectively. From TABLE 1 and TABLE 2, it can be seen that the proposed EFGD model has the best overall performance in terms of PLCC, SROCC and RMSE for both databases. In other words, on the SIQAD database, the overall performance of the first place is obtained compared to other state-of-the-art full reference image quality assessment models, and the overall performance of the first place is also obtained on the SCID database.

In addition, TABLE 1 and TABLE 2 also provide performance comparisons of the IQA models for each type of distortion. Experimental results recorded in TABLE 1 show that the proposed EFGD model is superior to most of sophisticated models in the SIQAD database, because it has the most and best performance in the various distortion types. It gets the best performance for three distortion types: GB, MB and JPEG. From TABLE 2, we can see that for the SCID database, the EFGD model for the JEPG distortion also has the highest performance. Although the EFGD does not achieve the best performance on other distortion types, its overall correlation on the SCID database is the highest.

In fact, the experiment results can be expected, due to the noise type that are blurred and compressed will inevitably reduce edges and let significant changes to the extracted edge information [30]. Despite the encouraging results of the EFGD model, its performance in contrast change (CC) is relatively poor.

TABLE 1. Performance comparisons of different IQA models experimented on the SIQAD database.

Criteria	Distortions	PSNR	SSIM [5]	IWSSIM [8]	VIF [13]	MAD [39]	FSIM [6]	GSIM [7]	GMSD [10]	VSI [12]	SCQI [40]	SIQM [29]	SPQA [1]	SQI [28]	SQMS [41]	ESIM [30]	SVQI [42]	GFM [32]	EFGD
PLCC	GN	0.9053	0.8806	0.8804	0.9011	0.8852	0.7428	0.8448	0.8956	0.8762	0.8807	0.8921	0.8921	0.8829	0.8986	0.8891	0.9031	0.8990	0.8757
	GB	0.8603	0.9014	0.9079	0.9102	0.9120	0.7206	0.8831	0.9094	0.8502	0.8535	0.9124	0.9058	0.9202	0.9126	0.9234	0.9132	0.9143	0.9315
	MB	0.7044	0.8060	0.8414	0.8490	0.8361	0.6874	0.7711	0.8436	0.662	0.6949	0.8565	0.8315	0.8789	0.8654	0.8886	0.8722	0.8662	0.9119
	CC	0.7401	0.7435	0.8404	0.7076	0.3933	0.7507	0.8077	0.7827	0.7723	0.7119	0.7902	0.7992	0.7724	0.8022	0.7641	0.8087	0.8107	0.8237
	JPEG	0.7545	0.7487	0.7998	0.7986	0.7662	0.5566	0.6778	0.7746	0.7124	0.6782	0.7717	0.7696	0.8218	0.785	0.7999	0.7953	0.8398	0.8470
	J2K	0.7893	0.7749	0.8040	0.8205	0.8344	0.6675	0.7242	0.8509	0.7479	0.7225	0.7940	0.8252	0.8271	0.8261	0.7888	0.8342	0.8486	0.8257
	LSC	0.7805	0.7307	0.8155	0.8385	0.8184	0.5964	0.7218	0.8559	0.7454	0.7418	0.7204	0.7958	0.8310	0.8119	0.7915	0.8283	0.8288	0.7895
	Overall	0.5858	0.7561	0.6519	0.8083	0.5467	0.5888	0.5659	0.7291	0.5543	0.6026	0.8520	0.8584	0.8644	0.8870	0.8788	0.8908	0.8828	0.8993
SROCC	GN	0.8790	0.8694	0.8743	0.8888	0.8721	0.7373	0.8404	0.8856	0.8655	0.8821	0.8711	0.8823	0.8602	0.8860	0.8757	0.8909	0.8795	0.8666
	GB	0.8573	0.8921	0.9060	0.9059	0.9087	0.7286	0.8796	0.9119	0.8495	0.8463	0.9102	0.9017	0.9244	0.9119	0.9239	0.9129	0.9132	0.9374
	MB	0.713	0.8041	0.8421	0.8492	0.8357	0.6641	0.7753	0.8441	0.7658	0.7604	0.8401	0.8255	0.881	0.8695	0.8938	0.8753	0.8699	0.9129
	CC	0.6828	0.6405	0.7563	0.6433	0.3907	0.7175	0.7148	0.6378	0.6495	0.5780	0.7055	0.6154	0.6677	0.6949	0.6108	0.7131	0.7038	0.7617
	JPEG	0.7569	0.7576	0.7978	0.7924	0.7674	0.5879	0.6796	0.7712	0.7196	0.7080	0.7754	0.7673	0.8189	0.7893	0.7989	0.7925	0.8434	0.8458
	J2K	0.7746	0.7603	0.7998	0.8131	0.8382	0.6363	0.7125	0.8436	0.7299	0.7231	0.7771	0.8152	0.8169	0.8194	0.7827	0.8282	0.8444	0.8164
	LSC	0.793	0.7371	0.8214	0.8463	0.8154	0.5979	0.7145	0.8592	0.7419	0.7588	0.7255	0.8003	0.8432	0.8293	0.7958	0.8412	0.8445	0.7927
	Overall	0.5570	0.7566	0.6546	0.8069	0.5831	0.5824	0.5483	0.7305	0.5381	0.6113	0.8450	0.8416	0.8548	0.8803	0.8632	0.8836	0.8735	0.8901
RMSE	GN	6.3372	7.0679	7.7044	6.4673	6.9391	9.9860	7.9811	6.6354	7.1890	7.0651	7.0165	6.7394	-	6.5461	6.8272	6.4044	6.6835	7.2017
	GB	7.7376	6.5701	6.3619	6.2859	6.2269	10.523	8.2788	6.9816	9.7450	9.3502	5.8367	6.4301	-	6.2113	5.8270	6.1550	6.1459	5.5185
	MB	9.2287	7.6967	7.0600	6.8704	7.1322	9.4432	8.2788	6.9816	9.7450	9.3502	6.0869	7.2223	-	6.5254	5.9639	6.3604	6.5184	5.3354
	CC	8.4591	8.4116	6.8184	8.8876	11.565	8.3190	7.416	7.8297	7.9900	8.8342	8.1079	7.6184	-	7.5098	8.1141	7.3996	7.3638	7.1324
	JPEG	6.1665	6.2295	5.6406	5.6551	6.038	7.8072	6.9085	5.9427	6.5950	6.9057	5.6548	6.0000	-	5.8210	5.6401	5.6969	5.1009	4.9944
	J2K	6.3819	6.5691	6.1804	5.9412	5.7276	7.7404	7.1675	5.4591	6.8990	7.1859	6.082	5.8706	-	5.8568	6.3877	5.7309	5.4985	5.8637
	LSC	5.3336	5.8253	4.9379	4.6497	4.9025	6.8486	5.9046	4.4121	5.6880	5.7226	5.3576	5.1664	-	4.9813	5.2150	4.7751	4.7736	5.2362
	Overall	11.601	9.3680	10.855	8.4282	11.986	11.570	11.801	9.7972	11.915	11.423	7.4936	7.3421	7.1982	6.6110	6.8310	6.5030	6.7234	6.2595

C. STEP-BY-STEP PERFORMANCE COMPARISON AND ANALYSIS

In this section, we will verify the accuracy of the EFGD model by the experimental results of each step. Firstly, we study the contributions of the feature extraction of edge sharpness map (ESM), edge brightness contrast map (EBCM) and edge chrominance map (ECM) on SIQAD and SCID databases. It is used to analyze the contribution of each edge feature to the performance of the algorithm. This work is accomplished by assigning different parameter values to equation (17). Specifically, the performance of edge sharpness map (ESM) can be obtained by making $\theta = 0$ and $\gamma = 1$. Then let $\theta = 1, \gamma = 0$ to get the edge brightness contrast map (EBCM) and edge chrominance map (ECM) performance by controlling the value of the parameter β. When $\beta = 1$, the performance of edge brightness contrast map (EBCM) can be obtained. When $\beta = 0$, the edge chrominance map (ECM) performance can be obtained. The corresponding results are recorded in TABLE 3.

Then, according to the last step of the algorithm, we choose a combination of two from these three features and compare the performance of the ''combination''. This work can also assign different parameter values to Eq. (17) to realize the performance of each part. When $\beta = 0, \theta = \gamma = 1$, the edge sharpness map (ESM) and edge chrominance map (ECM) fusion performance is obtained. When $\beta = 1, \theta = \gamma = 1$, the edge sharpness map (ESM) and edge brightness contrast map (EBCM) fusion is obtained. It is noteworthy that the performance of edge brightness contrast and edge chrominance is obtained by extracting two features and merging them respectively. The corresponding results are recorded in TABLE 4, where the symbol ''+'' denotes a combination of two edge features.

In addition, we test the effect of the parameter v in Eq. (18) in the adaptive algorithm, which is used to control the weight coefficient β on the two databases with different noise types. The detail distribution intervals of v for each distortion type are counted and the corresponding results are recorded in TABLE 5. By comparing the distribution interval of different noise types, we can find that in SIQAD and SCID, the value of v in most types of noise distribution is mainly concentrated in $[0.31 \sim 0.71]$. Only in the case of the CSC noise type, the value of v exceeds 0.71. We divide the value of v into three ranges. When v is greater than interval of different noise types, we can find that in SIQAD and SCID, the value of v in most types of noise distribution is mainly concentrated in $[0.31 \sim 0.71]$. Only in the case of the CSC noise type, the value of v exceeds 0.71. We divide the value of v into three ranges. When v is greater than 0.71, it can only be affected by the noise type CSC, so we increase the weight of the edge chrominance map (ECM), so that $\beta = 0.3$. When v is in $[0.31 \sim 0.71]$, we increased the weight of the edge brightness contrast map (EBCM), so that $\beta = 0.7$. For the rest of the values, after testing on two databases: SIQAD and SCID, we finally decided to make $\beta = 0.4$.

TABLE 2. Performance comparisons of different IQA models experimented on the SCID database.

Criteria	Distortions	PSNR	SSIM [5]	IWSSIM [8]	VIF [13]	MAD [39]	FSIM [6]	GSIM [7]	GMSD [10]	VSI [12]	SCQI [40]	SIQM [29]	SPQA [1]	SQI [28]	SQMS [41]	ESIM [30]	SVQI [42]	GFM [32]	EFGD
PLCC	GN	0.9530	0.9354	0.9431	0.9699	0.9315	0.9516	0.9170	0.9273	0.9556	0.9319	0.9269	-	-	0.9298	0.9563	0.9362	0.9497	0.9490
	GB	0.7772	0.8711	0.9174	0.8999	0.8559	0.8493	0.8449	0.7348	0.8307	0.8244	0.9266	-	-	0.9081	0.8700	0.9130	0.9156	0.9087
	MB	0.7615	0.8794	0.9055	0.8421	0.8362	0.8523	0.8383	0.7954	0.8177	0.8147	0.9152	-	-	0.8968	0.8824	0.8997	0.9023	0.8938
	CC	0.7435	0.6903	0.8989	0.8092	0.4987	0.8947	0.8675	0.8041	0.8093	0.8353	0.7821	-	-	0.8441	0.7908	0.8266	0.8787	0.8579
	JPEG	0.8393	0.8581	0.9308	0.9418	0.9251	0.9419	0.9373	0.9351	0.9148	0.9036	0.9226	-	-	0.9302	0.9421	0.9356	0.9392	0.9493
	J2K	0.9176	0.8586	0.9195	0.9489	0.9381	0.9607	0.9441	0.9422	0.9451	0.9312	0.9076	-	-	0.9468	0.9457	0.9513	0.9226	0.9446
	CSC	0.0622	0.0890	0.0527	0.0898	0.1296	0.0966	0.056	0.0952	0.9119	0.8393	0.0683	-	-	0.0628	0.0694	0.0919	0.8728	0.7943
	HEVC-SCC	0.7991	0.7914	0.8883	0.8656	0.8953	0.9228	0.8835	0.9043	0.9035	0.8708	0.8316	-	-	0.8515	0.9108	0.8496	0.8740	0.8852
	CQD	0.9210	0.7810	0.8930	0.9085	0.9014	0.9202	0.8974	0.9177	0.8873	0.8823	0.8385	-	-	0.8986	0.9005	0.9047	0.8928	0.9000
	Overall	0.7622	0.7343	0.7877	0.8200	0.7736	0.7718	0.7042	0.8337	0.7694	0.7489	0.8303	-	-	0.8557	0.8630	0.8604	0.8760	0.8846
SROCC	GN	0.9424	0.9171	0.9305	0.9616	0.9262	0.9378	0.9112	0.9341	0.9455	0.9556	0.9133	-	-	0.9155	0.9460	0.9191	0.9370	0.9395
	GB	0.7702	0.8698	0.9165	0.8954	0.8603	0.8476	0.8420	0.7931	0.8221	0.8638	0.9232	-	-	0.9079	0.8699	0.9079	0.9081	0.9053
	MB	0.7375	0.8588	0.8918	0.8259	0.8296	0.8370	0.8194	0.8148	0.8013	0.8587	0.9006	-	-	0.8814	0.8608	0.8842	0.8892	0.8690
	CC	0.7265	0.6564	0.8475	0.6115	0.4784	0.8473	0.8204	0.5672	0.8158	0.7465	0.7435	-	-	0.8027	0.6182	0.7705	0.8225	0.7839
	JPEG	0.8321	0.8490	0.9275	0.9349	0.9242	0.9403	0.9366	0.9344	0.9142	0.9171	0.9158	-	-	0.9236	0.9455	0.9287	0.9281	0.9435
	J2K	0.9074	0.8439	0.9067	0.9369	0.9330	0.9484	0.9349	0.9279	0.9307	0.9270	0.8935	-	-	0.9320	0.9359	0.9367	0.9085	0.9329
	CSC	0.0908	0.0963	0.1336	0.1221	0.1440	0.1182	0.1214	0.1165	0.9141	0.8970	0.0617	-	-	0.0814	0.1037	0.079	0.8736	0.7935
	HEVC-SCC	0.8074	0.8263	0.8867	0.8580	0.8771	0.9098	0.8730	0.8958	0.8929	0.8721	0.8517	-	-	0.8667	0.9036	0.8665	0.8712	0.8896
	CQD	0.9080	0.7766	0.8846	0.8918	0.9024	0.9031	0.8707	0.9047	0.8820	0.9099	0.8301	-	-	0.8913	0.8868	0.8957	0.8907	0.8868
	Overall	0.7512	0.7146	0.7714	0.7969	0.7576	0.7550	0.6945	0.8138	0.7621	0.7814	0.8086	-	-	0.8320	0.8478	0.8386	0.8759	0.8774
RMSE	GN	3.8093	4.4458	4.1780	3.0629	4.5714	3.8613	5.0127	4.7044	3.7138	4.5600	4.8222	-	-	4.6250	3.6760	4.4179	3.9378	3.9633
	GB	6.6633	5.1998	4.2163	4.6179	5.4775	5.5903	5.6648	7.1821	5.8956	5.9943	4.0989	-	-	4.4336	5.2213	4.3194	4.2566	4.4194
	MB	7.0843	5.2044	4.6376	5.8960	5.9947	5.7180	5.9607	6.6249	6.2922	6.3394	4.7388	-	-	4.8352	5.1431	4.7709	4.6121	4.9050
	CC	5.9867	6.4767	3.9218	5.2594	7.759	3.9979	4.4524	5.3211	5.2583	4.9217	6.1281	-	-	4.7995	5.4790	5.0374	4.2732	4.5989
	JPEG	8.1718	7.7179	5.4930	5.0536	5.7076	5.0471	5.2369	5.3275	6.0971	6.439	6.7341	-	-	5.5181	5.0373	5.3053	5.2011	4.7266
	J2K	6.3222	8.1562	6.2555	5.0207	5.5103	4.4180	5.2462	5.3283	5.2451	5.8002	7.2951	-	-	5.1191	5.1695	4.9058	6.1385	5.2201
	CSC	9.8203	9.8003	9.8257	9.7996	9.7564	9.7933	9.8239	9.7947	4.0392	5.3503	9.8394	-	-	9.8199	9.8156	9.7977	4.8031	5.9775
	HEVC-SCC	8.4009	8.5037	6.3904	6.9657	6.1988	5.3583	6.5176	5.9393	5.9628	6.8407	8.1970	-	-	7.2938	5.7446	7.3381	6.7590	6.4720
	CQD	4.9814	7.9855	5.7530	5.3440	5.5354	5.0054	5.6406	5.0796	5.8964	6.0188	7.1976	-	-	5.6110	5.5607	5.4481	5.7592	5.5725
	Overall	9.1682	9.6133	8.7243	8.1069	8.9739	9.0047	10.055	7.8210	9.0456	9.3846	7.8920	-	-	7.3276	7.1552	7.2178	6.8310	6.6044

TABLE 3. Performance of three edge features on SIQAD and SCID database.

Database	Criteria	ESM	EBCM	ECM
SIQAD	PLCC	0.8297	0.7431	0.4833
	SROCC	0.8116	0.7124	0.4754
	RMSE	7.7941	9.5784	12.5312
SCID	PLCC	0.8007	0.7216	0.6102
	SROCC	0.7863	0.7068	0.6055
	RMSE	8.2672	9.8043	11.2197

TABLE 4. Performance of two edge feature map combinations on SIQAD and SCID database.

Database	Criteria	ESM+ECM	ESM+EBC	EC+EBCM
SIQAD	PLCC	0.7889	0.8399	0.7392
	SROCC	0.7874	0.8237	0.7122
	RMSE	8.7956	7.7685	9.6409
SCID	PLCC	0.8348	0.7533	0.7730
	SROCC	0.8297	0.6893	0.7728
	RMSE	7.7976	9.3147	8.9885

Finally, in order to verify the feasibility of combining in gradient domain with image feature in this algorithm, we calculate the performance of image feature extraction directly from image pixel domain and the comparison results are recorded in TABLE 6.

Through the above experimental results, we not only verify the feasibility of the algorithm, but also get the following conclusions: the ESM and EBCM contribute much more to the proposed EFGD model than the edge chrominance map (ECM). This is due to the edge sharpness map (ESM) and the edge brightness contrast map (EBCM) are extracted in the image luminance channel, and the HVS is more sensitive to the image luminance channels. But the EFGD model can ultimately achieve better performance, which is still inseparable from the role of the chrominance component.

D. COMPUTATIONAL COMPLEXITY COMPARISON

Computational complexity is also an important indicator when comparing different IQA models in practical application. So that the average running time of one image is measured for each IQA model by testing on the SCID database (1,800 distorted SCIs with resolution of 1280×720). To have a fair comparison, all the source codes of tested IQA models are obtained from their authors or websites and are performed

TABLE 5. Distribution interval of index *v* for different noise types in the two databases.

Database	Distortions	interval
SIQAD	GN	[0.56,0.70]
	GB	[0.36,0.64]
	MB	[0.47,0.63]
	CC	[0.40,0.77]
	JPEG	[0.55,0.69]
	J2K	[0.48,0.69]
	LSC	[0.57,0.69]
SCID	GN	[0.34,0.71]
	GB	[0.38,0.70]
	MB	[0.31,0.67]
	CC	[0.40,0.72]
	JPEG	[0.40,0.71]
	J2K	[0.43,0.71]
	CSC	[0.71.0.72]
	HEVC-SCC	[0.52,0.72]
	CQD	[0.55,0.72]

TABLE 6. Performance comparison of edge features on gradient domain and image pixel domain on SIQAD and SCID database.

Database	Criteria	Image pixel domain	Gradient domain
SIQAD	PLCC	0.8879	0.8993
	SROCC	0.8767	0.8901
	RMSE	6.5836	6.2595
SCID	PLCC	0.8748	0.8846
	SROCC	0.8676	0.8774
	RMSE	6.8260	6.6044

TABLE 7. Computational complexity comparison of different IQA models, measured in seconds per frame (*spf*).

Model	Time cost (*spf*)	Model	Time cost (*spf*)
MAD[39]	3.6659	SIQM[29]	0.2245
VIF[13]	2.3065	SQMS[41]	0.1867
SSIM[5]	0.1096	ESIM[30]	2.6201
FSM[6]	0.3896	EFGD	1.9881

under the same test procedure and environment. The computer used is equipped with an E5-1603 CPU@2.8GHz with 32GBs of RAM, and the software platform is Matlab R2016a. The run-time results are documented in TABLE 7. It can be observed that the proposed EFGD model get a relatively low computational complexity.

IV. CONCLUSION

In this paper, we propose a new screen content image (SCI) quality assessment model (EFGD). The novelty of the EFGD model is that the proposed edge features (e.g., edge sharpness, edge brightness/ contrast and edge chrominance) are all extracted from the gradient map of input SCIs. The obtained edge features in gradient domain can well consistent with the visual characteristics of the HVS. Three similarity maps based on these edge features are constructed, and then fused by an adaptive weighting strategy. The proposed weighting algorithm takes account of the statistical distribution of collected SCIs, which can reveal the effect of features. Finally, the edge sharpness pooling strategy is used to compute the final evaluation score. Experimental tests on two general large SCI databases show that the proposed EFGD model gets the highest performance compared to other advanced IQA models and prove the effectiveness of extracted edge features in the gradient domain.

REFERENCES

[1] H. Yang, Y. Fang, and W. Lin, "Perceptual quality assessment of screen content images," *IEEE Trans. Image Process.*, vol. 24, no. 11, pp. 4408–4421, Aug. 2015.
[2] S. Wang, L. Ma, Y. Fang, W. Lin, S. Ma, and W. Gao, "Just noticeable difference estimation for screen content images," *IEEE Trans. Image Process.*, vol. 25, no. 8, pp. 3838–3851, May 2016.
[3] K. Gu, G. Zhai, W. Lin, X. Yang, and W. Zhang, "Learning a blind quality evaluation engine of screen content images," *Neuro Comput.*, vol. 196, pp. 140–149, Jul. 2016.
[4] B. Girod, "What's wrong with mean-squared error?" in *Digital Images and Human Vision*. Cambridge, MA, USA: MIT Press, 1993, pp. 207–220.
[5] Z. Wang, A. C. Bovik, H. R. Sheikh, and E. P. Simoncelli, "Image quality assessment: From error visibility to structural similarity," *IEEE Trans. Image Process.*, vol. 13, no. 4, pp. 600–612, Apr. 2004.
[6] L. Zhang, L. Zhang, X. Mou, and D. Zhang, "FSIM: A feature similarity index for image quality assessment," *IEEE Trans. Image Process.*, vol. 20, no. 8, pp. 2378–2386, Aug. 2011.
[7] A. Liu, W. Lin, and M. Narwaria, "Image quality assessment based on gradient similarity," *IEEE Trans. Image Process.*, vol. 21, no. 4, pp. 1500–1512, Apr. 2012.
[8] Z. Wang and Q. Li, "Information content weighting for perceptual image quality assessment," *IEEE Trans. Image Process.*, vol. 20, no. 5, pp. 1185–1198, May 2011.
[9] X. Zhang, X. Feng, W. Wang, and W. Xue, "Edge strength similarity for image quality assessment," *IEEE Signal Process. Lett.*, vol. 20, no. 4, pp. 319–322, Apr. 2013.
[10] W. Xue, L. Zhang, X. Mou, and A. C. Bovik, "Gradient magnitude similarity deviation: A highly efficient perceptual image quality index," *IEEE Trans. Image Process.*, vol. 23, no. 2, pp. 684–695, Feb. 2014.
[11] H. Z. Nafchi, A. Shahkolaei, R. Hedja, and M. Cheriet, "Mean deviation similarity index: Efficient and reliable full-reference image quality evaluator," *IEEE Access*, vol. 4, pp. 5579–5590, 2016.
[12] L. Zhang, Y. Shen, and H. Li, "VSI: A visual saliency-induced index for perceptual image quality assessment," *IEEE Trans. Image Process.*, vol. 23, no. 10, pp. 4270–4281, Aug. 2014.
[13] H. R. Sheikh and A. C. Bovik, "Image information and visual quality," *IEEE Trans. Image Process.*, vol. 15, no. 2, pp. 430–444, Feb. 2006.
[14] H. R. Sheikh, A. C. Bovik, and G. de Veciana, "An information fidelity criterion for image quality assessment using natural scene statistics," *IEEE Trans. Image Process.*, vol. 14, no. 12, pp. 2117–2128, Dec. 2005.
[15] L. Li, Y. Yan, Z. Lu, J. Wu, K. Gu, and S. Wang, "No-reference quality assessment of deblurred images based on natural scene statistics," *IEEE Access*, vol. 5, pp. 2163–2171, 2017.
[16] H. Gao, Q. Miao, J. Yang, and Z. Ma, "Image quality assessment using image description in information theory," *IEEE Access*, vol. 6, pp. 47181–47188, 2018, doi: 10.1109/ACCESS.2018.2832722.
[17] Z. Wang, E. P. Simoncelli, and A. C. Bovil, "Multi-scale structural similarity for image quality assessment," in *Proc. IEEE Conf. Signals Syst. Comput.*, vol. 2, Nov. 2003, pp. 1398–1402.
[18] F. Gao, D. Tao, X. Gao, and X. Li, "Learning to rank for blind image quality assessment," *IEEE Trans. Neural Netw. Learn. Syst.*, vol. 26, no. 10, pp. 2275–2290, Oct. 2015.
[19] T.-J. Liu, K.-H. Liu, J. Y. Lin, W. Lin, and C.-C. J. Kuo, "A ParaBoost method to image quality assessment," *IEEE Trans. Neural Netw. Learn. Syst.*, vol. 28, no. 1, pp. 107–121, Jan. 2017.
[20] S. Wang, C. Deng, W. Lin, G. Huang, and B. Zhao, "NMF-based image quality assessment using extreme learning machine," *IEEE Trans. Cybern.*, vol. 47, no. 1, pp. 232–243, Jan. 2017.
[21] Y. Ding *et al.*, "No-reference stereoscopic image quality assessment using convolutional neural network for adaptive feature extraction," *IEEE Access*, vol. 6, pp. 37595–37603, 2018.

[22] W. Hou, X. Gao, D. Tao, and X. Li, "Blind image quality assessment via deep learning," *IEEE Trans. Neural Netw. Learn. Syst.*, vol. 26, no. 6, pp. 1275–1286, Jun. 2015.
[23] W. Zhang, C. Qu, L. Ma, J. Guan, and R. Huang, "Learning structure of stereoscopic image for no-reference quality assessment with convolutional neural network," *Pattern Recognit.*, vol. 59, pp. 176–187, Nov. 2016.
[24] F. Gao, Y. Wang, P. Li, M. Tan, J. Yu, and Y. Zhu, "DeepSim: Deep similarity for image quality assessment," *Neurocomputing*, vol. 257, pp. 104–114, Sep. 2017.
[25] H. Wang, J. Fu, W. Lin, S. Hu, C.-C. J. Kuo, and L. Zuo, "Image quality assessment based on local linear information and distortion-specific compensation," *IEEE Trans. Image Process.*, vol. 26, no. 2, pp. 915–926, Feb. 2017.
[26] L. Tang, Q. Wu, W. Li, and Y. Liu, "Deep saliency quality assessment network with joint metric," in *IEEE Access*, vol. 6, pp. 913–924, 2018, doi: 10.1109/ACCESS.2017.2776344.
[27] Y. Ding *et al.*, "No-reference stereoscopic image quality assessment using convolutional neural network for adaptive feature extraction," *IEEE Access*, vol. 6, pp. 37595–37603, 2018.
[28] S. Wang, K. Gu, K. Zeng, Z. Wang, and W. Lin, "Objective quality assessment and perceptual compression of screen content images," *IEEE Comput. Graph. Appl.*, vol. 38, no. 1, pp. 47–58, Jan./Feb. 2018, doi: 10.1109/MCG.2016.46.
[29] K. Gu, S. Wang, G. Zhai, S. Ma, and W. Lin, "Screen image quality assessment incorporating structural degradation measurement," in *Proc. IEEE Int. Symp. Circuits Syst.*, May 2015, pp. 125–128.
[30] Z. Ni, L. Ma, H. Zeng, J. Chen, C. Cai, and K.-K. Ma, "ESIM: Edge similarity for screen content image quality assessment," *IEEE Trans. Image Process.*, vol. 26, no. 10, pp. 4818–4831, Oct. 2017.
[31] Y. Fang, J. Yan, J. Liu, S. Wang, Q. Li, and Z. Guo, "Objective quality assessment of screen content images by uncertainty weighting," *IEEE Trans. Image Process.*, vol. 26, no. 4, pp. 2016–2027, Apr. 2017.
[32] Z. Ni, H. Zeng, L. Ma, J. Chen, C. Cai, and K.-K. Ma, "A Gabor feature-based quality assessment model for the screen content images," *IEEE Trans. Image Process.*, vol. 27, no. 9, pp. 4516–4528, Sep. 2018, doi: 10.1109/TIP.2018.2839890.
[33] J. Sun, J. Sun, Z. Xu, and H.-Y. Shum, "Gradient profile prior and its applications in image super-resolution and enhancement," *IEEE Trans. Image Process.*, vol. 20, no. 6, pp. 1529–1542, Jun. 2011.
[34] M. A. Stricker and M. Orengo, "Similarity of Color Images," *Proc. SPIE*, vol. 2420, pp. 381–392, Mar. 1995.
[35] L. Yitao *et al.*, "The application study on the improved canny algorithm for edge detection in fundus image," in *Software Engineering and Knowledge Engineering: Theory and Practice*. Berlin, Germany: Springer, 2012.
[36] X. Lu, H. Zeng, J. Chen, J. Zhu, C. Cai, and K.-K. Ma, "Multi-exposure image fusion quality assessment using contrast information," in *Proc. Int. Symp. Intell. Signal Process. Commun. Syst.*, Nov. 2017, pp. 34–38.
[37] VQEG. (Aug. 2015). *Final Report From the Video Quality Experts Group on the Validation of Objective Models of Video Quality Assessment*. [Online]. Available: http://www.its.bldrdoc.gov/vqeg/vqeg-home.aspx
[38] H. R. Sheikh, M. F. Sabir, and A. C. Bovik, "A statistical evaluation of recent full reference image quality assessment algorithms," *IEEE Trans. Image Process.*, vol. 15, no. 11, pp. 3440–3451, Nov. 2006.
[39] E. C. Larson and D. M. Chandler, "Most apparent distortion: Full-reference image quality assessment and the role of strategy," *J. Electron. Imag.*, vol. 19, no. 1, pp. 011006-1–011006-21, 2010.
[40] S.-H. Bae and M. Kim, "A novel image quality assessment with globally and locally consilient visual quality perception," *IEEE Trans. Image Process.*, vol. 25, no. 5, pp. 2392–2406, May 2016.
[41] K. Gu *et al.*, "Saliency-guided quality assessment of screen content images," *IEEE Trans. Multimedia*, vol. 18, no. 6, pp. 1098–1110, Jun. 2016.
[42] K. Gu, J. Qiao, X. Min, G. Yue, W. Lin, and D. Thalmann, "Evaluating quality of screen content images via structural variation analysis," *IEEE Trans. Vis. Comput. Graphics*, vol. 24, no. 10, pp. 2689–2701, Oct. 2018, doi: 10.1109/TVCG.2017.2771284.

RUIFENG WANG received the B.E degree from the Shandong University of Science and Technology, Jinan, China. He is currently pursuing the M.E degree with the School of Computer Science and Technology, Qingdao University, Qingdao, China. His research interests include image quality assessment and machine learning.

HUAN YANG received the B.S. degree in computer science from the Heilongjiang Institute of Technology, China, in 2007, the M.S. degree in computer science from Shandong University, China, in 2010, and the Ph.D. degree in computer engineering from Nanyang Technological University, Singapore, in 2015. She is currently a Lecturer with the College of Computer Science and Technology, Qingdao University, Qingdao, China. Her research interests include image/video processing and analysis, perception-based modeling and quality assessment, object detection/recognition, and machine learning.

ZHENKUAN PAN received the B.E. degree from Northwestern Polytechnical University, Xian, China, in 1987, and the Ph.D. degree from Shanghai Jiao Tong University, Shanghai, China, in 1992. He is currently a Professor with the College of Computer Science and Technology, Qingdao University, Qingdao, China. He has authored or co-authored more than 300 academic papers in the areas of computer vision, dynamics, and control. His research interests include variational models of image and geometry processing and multibody system dynamics.

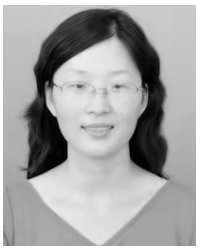

BAOXIANG HUANG received the B.S. degree in traffic engineering from the Shandong University of Technology, China, in 2002, the M.S. degree in mechatronic engineering from Shandong University, China, in 2005, and the Ph.D. degree in computer engineering from the Ocean University of China, China. She is currently an Associate Professor with the College of Computer Science and Technology, Qingdao University, Qingdao, China. Her research interests include remote sensing image processing and analysis, urban acoustic environment modeling, and quality assessment.

GUOJIA HOU received the B.S. degree in computer science and the M.S. and Ph.D. degrees in computer applications technology from the Ocean University of China, in 2010, 2012, and 2015, respectively. He is currently a Lecturer with the College of Computer Science and Technology, Qingdao University. He has authored more than 10 journal and conference papers. His current research interests include image processing, image quality evaluation, and pattern recognition.